Physics and Chemistry of the Earth 66 (2013) 60–67

Contents lists available at ScienceDirect

Physics and Chemistry of the Earth

journal homepage: www.elsevier.com/locate/pce

Dechlorination of 3,3′,4,4′-tetrachlorobiphenyl (PCB77) in water, by nickel/iron nanoparticles immobilized on L-lysine/PAA/PVDF membrane

Bonani Seteni [a], Jane Catherine Ngila [a,*], Keneiloe Sikhwivhilu [b], Richard M. Moutloali [b], Bhekie Mamba [a]

[a] Department of Applied Chemistry, University of Johannesburg, Doornfontein Campus, P.O. Box 17011, Doornfontein 2028, Johannesburg, South Africa
[b] Advanced Materials Division, DST/Mintek Nanotechnology Innovation Centre, Mintek, 200 Malibongwe drive, Randburg 2125, Johannesburg, South Africa

ARTICLE INFO

Article history:
Available online 2 September 2013

Keywords:
Bimetallic Ni/Fe nanoparticles
Dechlorination
PCB77
Chlorinated compounds in water
PVDF/membrane

ABSTRACT

In this study, the dechlorination of chlorinated hydrocarbon 3,3′,4,4′-tetrachlorobiphenyl (PCB77) by bimetallic Ni/Fe nanoparticles immobilized on L-lysine/PAA/PVDF membrane was investigated at ambient conditions through the batch mode operation. The membrane support polyvinylidene fluoride (PVDF) was modified by *in situ* polymerization of acrylic acid in aqueous phase, then L-lysine was covalently bonded to the polymerized acrylic acid chains with the aid of a water-soluble carbodiimide, 1-ethyl-3-(3-dimethylaminopropyl)-carbodiimide hydrochloride (EDC). The modification procedure involved cationic ion exchange with Fe^{2+}, reduction to Fe^0 with $NaBH_4$ and finally deposition of Ni^0. The scanning electron microscopic images showed that the Ni/Fe nanoparticles were successfully immobilized inside the membrane using the polyacrylic acid (PAA) as an inter-linkage between PVDF and L-lysine. A systematic characterization of the composite was performed using ATR-FTIR, HRSEM, EDX, HRTEM, XRD, and contact angle measurement studies and a relatively uniform distribution of Ni/Fe was found in L-lysine/PAA/PVDF membrane because of its hydrophilic nature. The obtained Ni/Fe nanoparticles consist of Fe^0 core surrounded by the Ni^0 shell. The diameter of Ni/Fe nanoparticles was predominantly within the range 20–30 nm. The immobilized Ni/Fe nanoparticles exhibited a good reactivity towards the dechlorination of the chlorinated hydrocarbon since the concentration of the PCB77 was decreased by catalytic dechlorination with Ni/Fe nanoparticles inside the L-lysine/PAA/PVDF membrane. Dechlorination efficiency of 98% was achieved within 9 h.

1. Introduction

Over 780 million people in the world are still without access to improved sources of drinking water and 2.5 billion lack improved sanitation (WHO and UNICEF, 2012). This lack of access to safe water has a major impact on people's well-being as water is life to man and animals (Hoekstra, 2012). If appropriate measures are not taken, most of urban Africa currently confront or will be confronted by inadequate water supplies (UN-Habitat, 2011). There are several factors that contribute to the scarcity of water in the world, namely, droughts (Verones et al., 2010), poor sanitation and pollution, with the latter being the most prevalent (Berger and Finkbeiner, 2010). However, water pollution is one of the eminent human killers due to new alien diseases introduced into the environment that, which if bio-accumulated, can cause complexity in human health (WHO and UNICEF, 2012). This phenomenon has raised concern in the public for stringent environmental legislation and alternative technology in water treatment (UN-Water, 2012).

The presence of (free) dissolved chlorine used as a disinfectant in conventional water treatment plants is a concern (Hoekstra et al., 2012). Studies have found that chlorine reacts with residual natural organic matter (NOM) (Su et al., 2012). This reaction process can form disinfection by-products (DBPs) such as trihalomethanes e.g., chloroform, haloacetics and other halogenated organics (Pfister et al., 2011; Ridoutt and Pfister 2010a,b). DBPs are carcinogens, and direct exposure to high levels can lead to cancers, miscarriages or intersex (Su et al., 2012).

A concentration of only a few parts per million (ppm) of these possible chlorinated contaminants in water supplies require expensive pumps and treatment methods (Seol et al., 2011). As a result, significant scientific efforts have been directed toward the development of remediation processes, for these chlorinated persistent pollutants in affordable means. One of those strategies is the use of membranes embedded with catalytic nanoparticles.

Membranes are used for the separations based on solution diffusion and size exclusion (Ruhl et al., 2012). The modification of the membranes helps to extend their area of application toward advanced separations by development of biomaterials or catalysis (Grzelczak et al., 2010). In the field of catalysis in particular, there is a growing awareness in detoxification of organic chlorinated

* Corresponding author. Tel.: +27 11 5596197; fax: +27 11 5596425.
E-mail address: jcngila@uj.ac.za (J.C. Ngila).

1474-7065/$ - see front matter © 2013 Elsevier Ltd. All rights reserved.
http://dx.doi.org/10.1016/j.pce.2013.08.010

compounds from aqueous streams such as dams and rivers (Yoshimatsu et al., 2012). Chlorinated organic compounds constitute a large group of pollutants of international concern due to their high toxicity, and persistency in the environment (Mackenzie et al., 2012). Microfiltration membrane such as PVDF has been used for separation of substances due to its chemical and thermal stability (Man et al., 2011). The advancements in nanotechnology have conjoined with membrane technology to help reduce the availability of toxic chlorinated compounds such PCBs in drinking water through catalytic applications (Li et al., 2012). Over the last few years, various synthetic methods (Behari, 2010) have been attempted to produce bimetallic Ni/Fe nanoparticles (Gui et al., 2012), and introduce them onto the membrane surface and pores (He et al., 2012) so as to enhance the membranes efficiency for dechlorination purposes (Andersin et al., 2012). The function of the bimetallic couple is to act as a redox couple during dechlorination where the Fe is oxidized and liberates a hydrogen molecule (Saha et al., 2010). The latter is captured by Ni which acts as a catalyst and decomposes the H_2 molecule to hydrogen atoms. The latter in turn replaces the chlorine atom (Cl) from chlorinated organic matter (Gui et al., 2012). The challenge in using the bimetallic redox couple is mainly leaching out of the metals of the couple into the treated water (Yunqing et al., 2012). The challenge of leaching of the nanoparticles reverses the progress made on the treated water (Ramezani-Dakhel et al., 2013). To overcome this problem, our study introduced a monomer (e.g., L-lysine) that contains multifunctional chelating groups such as —OH, —NH_2 and —COOH which will be responsible for entrapping and evenly distribution of the nanoparticles within the pores and onto the surface of the membrane for the dechlorination purposes with minimum leaching (Parshetti and Doong, 2012).

In this study we report the synthesis and characterization of bimetallic Ni/Fe nanoparticles immobilized inside the L-lysine/PVDF composite. The attachment of the L-lysine on PVDF membranes was made possible by first polymerizing the acrylic acid inside the pores of the membranes since it was a supplier of —OH groups through the carboxylic functional group responsible for the adhesion of the L-lysine on PVDF membrane. The L-lysine was covalently bonded to the —OH group from —COOH with the aid of a carbodiimide, 1-ethyl-3-(3-dimethylaminopropyl) carbodiimide hydrochloride (EDC). The bimetallic Ni/Fe nanoparticles were entrapped by the membrane through the hydroxyl and the amine groups provided by the amino acid on the surface of the membrane. This reduces their agglomeration and enhances the reactivity of the product formed. The immobilized Ni/Fe nanoparticles were then applied for the dechlorination of the chlorinated hydrocarbon (PCB77) in water. The dechlorination efficiency and the rate of leaching of the nanoparticles were also investigated.

2. Experimental section

2.1. Materials and chemicals

All the solutions were prepared in double-distilled water. The reagents used were of analytical grade. Polyvinylidene fluoride (PVDF) membrane used in this study (47 mm disks, 0.2 μm pore size, Pall Corporation) possessed some degree of wetting (with a contact angle of 60.3 ± 5.0). Nickel (II) chloride hexahydrate ($NiCl_2 \cdot 6H_2O$) (99%), ferrous-sulphate heptahydrate ($FeSO_4 \cdot 7H_2O$) (98%) and sodium borohydride ($NaBH_4$) (95%) were supplied by Merck Chemicals (Johannesburg, South Africa). L-lysine ($C_6H_{14}N_2O_2$) (98%) was obtained from Sigma Aldrich. 3,3′,4,4′-tetrachlorobiphenyl (PCB77) (98.4%) and N-(3-dimethylaminopropyl)-N′-ethylcarbodimide hydrochloride (EDC) (98%) were bought from Sigma–Aldrich (St. Louis, USA). Acrylic acid (99%) stabilized with hydroquinone monomethyl ether for synthesis and ethanol (99.9%) both were obtained from Merck Chemicals.

2.2. Modification of PVDF membrane

The pores of PVDF membranes were functionalized with polyacrylic acid (PAA) by *in situ* polymerization of acrylic acid. The choice of the membrane materials can be used for this application, PVDF was due to its high chemical and thermal stabilities. The polymerization reaction was carried out in aqueous phase and the procedure was adapted from the literature by Huh et al. (2012). The polymerizing solution contained 30 wt% acrylic acid (monomer), ethylene glycol (cross-linker, added in a 1:6.5 M ratio of EG to acrylic acid), and 1 wt% potassium peroxodisulfate (initiator). The PVDF membrane was dipped in the polymerization solution for 2 min, sandwiched between two Teflon plates and placed in an oven at 90 °C for 4 h (Bhattacharyya et al., 2011). Temperature increase is necessary for the formation of ester bonds between the ethylene glycol cross-linker and carboxylates on the formed polyacrylate. Nitrogen gas was bubbled through to remove oxygen as oxidation inhibits the polymerization reaction.

2.3. Immobilization of the L-lysine

The hydrophilized membranes were soaked in a buffer solution containing a known quantity of EDC (0.03 M) at pH 3 to activate the carboxylic acid's hydroxyl group (—OH) attached to the membrane. This reaction was performed at 4 °C for a period of 4 h. The OH-activated membrane was then introduced in an L-lysine solution (20 mg/mL) maintained at pH 10 and 4 °C for 24 h to immobilize L-lysine on the membrane. The formed L-lysine/PVDF composite membrane was then washed in a buffer solution (pH 10) for 24 h to remove residual unreacted L-lysine and by-product, iso-urea. The composite membrane was then rinsed several times in deoxygenated water, dried in an oven at 60 °C and kept safe for the immobilization of bimetallic nanoparticles.

2.4. Bimetallic Ni/Fe nanoparticle synthesis

Prior to Fe^{2+} ion exchange, L-lysine coated PVDF membranes were immersed in NaCl (5–10 wt%) solution at pH 10 for 10 h to convert the —COOH to form COONa, and —NH to form —NNa (Smuleac et al., 2010). This was to minimize the pH effects on ion exchange equilibrium, thus enhancing the ion exchange capacity. The membrane was washed with deionised water and then immersed in a solution of 0.38 M $FeSO_4 \cdot 7H_2O$ in 200 mL of deoxygenated deionised water at pH of 4.8–5 for 12 h. Nitrogen gas was bubbled to minimize oxidation of Fe^{2+}. The reduction with $NaBH_4$ ensured Fe^0 nanoparticle formation, after which the membranes were stored in ethanol to prevent oxidation, see Eq. (1):

$$Fe^{2+} + 2BH_4^- + 6H_2O \rightarrow Fe^0 \downarrow + 2B(OH)_3 + 7H_2 \uparrow \quad (1)$$

The secondary metal, Ni, was deposited on the Fe nanoparticles by immersing the membrane (30 min – 1 h) in a 100 mM $NiCl_2 \cdot 6H_2O$ solution (50 mL) (in closed vials, vigorous shaking) of ethanol/ water (90:10 vol.% mixture), preventing the oxidation of the highly reactive Fe nanoparticles. This created core–shell nanoparticles. The deposition occurred via the well known redox reactions see Eq. (2):

$$Ni^{2+} + Fe^0 \rightarrow Fe^{2+} + Ni^0 \quad (2)$$

Unsupported nanoparticles were synthesized using the same procedure as stated above in the absence of the membrane. The purpose for the synthesis of the unsupported nanoparticles was to obverse their agglomeration as compared to the supported nanoparticles and evaluates their size.

The Ni/Fe modified membranes were washed three times with 100 mL ethanol to remove unreacted Boron and unattached Ni/Fe

nanoparticles on the membranes. The composites were then stored in ethanol until the use for dechlorination experiments.

2.5. Membrane and nanoparticle characterization

2.5.1. Fourier Transform Infrared (FT-IR) characterization

The Fourier Transform Infrared spectra of the bare, PAA-coated and L-lysine/PAA/PVDF membranes were recorded on a Bruker Tensor 27 FTIR with attenuated total reflectance (ATR). The PAA-coated PVDF membranes were dried at 90 °C for 4 h before analysis and L-lysine/PAA/PVDF membranes were dried at 60 °C for 1–2 h before the analysis. Data was collected using 60 scans at a resolution of 4 cm^{-1}. This was to confirm the presence of the functional groups in the modified and unmodified membranes.

2.5.2. The Field Emission Scanning Electron Microscopy (FESEM)

The Field Emission Scanning Electron Microscopy (FESEM) FEI Nova Nanosem 200 was used to determine the surface morphology of the modified membranes, granule size and the shape of the nanoparticles entrapped inside the pores of the membrane.

2.5.3. X-ray diffraction (XRD) characterization

Crystal structure was studied by D/MAX-RB X-ray diffraction (XRD) (Rigaku Company, Japan), 2-Theta range measurement, Cu Kα.

2.5.4. Elemental analysis with FESEM-energy dispersive X-ray spectroscopy (FESEM-EDS)

The elemental analysis of the composites was studied using FESEM (FEI Nova Nanosem 200) interfaced to EDS (Oxford Instrument, UK) as shown in Fig. 3.

2.5.5. Contact angle measurement confirmation

Data Physics, Contact angle measurement (CAM), OCA 15EC was used to confirm the hydrophilicity of the membranes.

2.5.6. Characterization by Transmission Electron Microscopy (HRTEM)

High Resolution Transmission Electron Microscopy (HRTEM), JEOL, JEM 2100 F was used to observe the granule size and the shape of the unsupported nanoparticles and compare their dispersion to the nanoparticles immobilized on the surface of the membrane and inside the pores of the membrane.

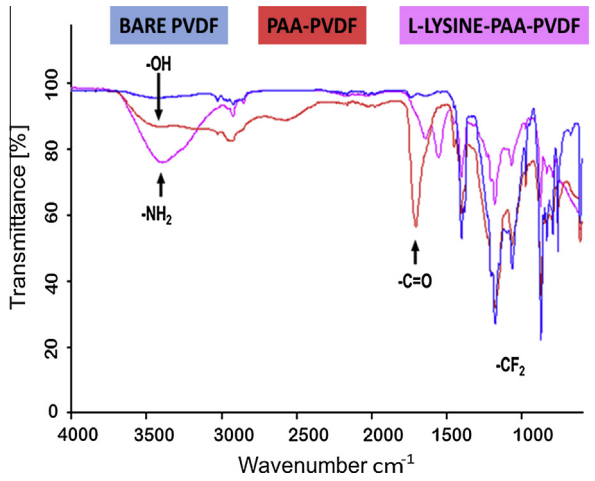

Fig. 1. ATR-FTIR for bare, PAA-functionalized and L-lysine–PAA–PVDF membrane.

2.6. Application studies of Ni/Fe/L-lysine/PAA/PVDF membrane for catalytic dechlorination of PCB77 in water using batch mode and detection with GC-GC-TOF/MS

Dechlorination reactions were carried out at room temperature in diffusive (batch) mode. The batch experiment for the dechlorination reaction of PCB77 was conducted in 50 mL glass vials by time series of sample sacrificial experiments. The L-lysine/PAA/PVDF MF membranes (each 17.3 cm^2 membrane was embedded with ~12.5 mg of Ni/Fe NPs), they were loaded into each reaction vial containing a 20 mL solution of PCB77 (5 mg L^{-1} in 50% (v/v) ethanol in water). The vials were sealed with Teflon-lined rubber septum cap immediately, and then placed on a rotary shaker at a speed of 170 rpm. Dechlorination experiments were conducted for 1–9 h. After the dechlorination experiments, the solution was extracted with 5 mL hexane for 12 h in a rotary shaker at the same speed used during dechlorination to attain extraction equilibrium.

3. Results and discussion

3.1. Characterization and optimization studies of the functionalized membrane

3.1.1. Fourier Transform Infrared (FT-IR) characterization

The modified and unmodified membranes were characterized with FTIR and the resulting spectra are presented in Fig. 1.

The shape of an absorption band can be helpful in identifying the compound responsible for an IR spectrum. The organic functionalities for the hydrophilized PVDF, PAA-coated and L-lysine bonded PVDF membranes were studied by ATR-FTIR spectroscopy as shown in Fig. 1a. The spectrum of the bare PVDF membrane exhibits some intensive bands at 1076, 835 cm^{-1}, which are assigned to the characteristic vibration of C—H and the strong absorption at wavenumbers 1140–1280 cm^{-1} characteristic of CF_2 found in PVDF (Smuleac et al., 2010). The PAA-coated PVDF membrane shows a peak at 1710 cm^{-1} which is not present in the spectrum for the bare PVDF membrane. This peak is due to the presence of C=O bond stretching in carboxylic acid groups (Gao et al., 2010). The PAA–PVDF composite spectrum has a characteristic absorption band at 3380 cm^{-1}. This confirms the presence of the —OH groups (Bieroza et al., 2010), indicating successful PAA immobilization within the functionalized membrane (Smuleac et al., 2010).

The polymerization reaction was carried out in a series of steps in the presence of a cross-linker, ethylene glycol. This is a bidentate molecule which can react with two —COOH groups at 90 °C cross-linking the PAA chains, thus preventing their leaching from the membrane (Bhattacharyya et al., 2011). Since ethylene glycol binds to carboxyl groups from PAA, the amount of cross-linking agent has to be kept low in order to maintain free —COOH groups required for the linkage of the L-lysine to the membrane through a covalent. After the treatment by EDC and L-lysine, new functional groups were observed on the PVDF surface, these being assigned to amine and carboxyl groups of the L-lysine. Both —OH and N—H bonds stretch at wavenumbers above 3100 cm^{-1}, but the shapes of their stretch bands are distinctive.

The presence of N—H bond after the reaction of an L-lysine and PAA is indicated by the peak at 3300 cm^{-1} in Fig. 1a, the signal is narrower and less intense than O—H absorption band (~3300 cm^{-1}) (Ezzaafrani et al., 2012). The —OH absorption band of carboxylic acid (~3300–2500 cm^{-1}) is broad than the —OH of an alcohol and amine (Nguyen et al., 2012). The intensity of an absorption band depends on the polarity of the bond (Ezzaafrani et al., 2012). The more polar the bond, the greater is the intensity of the absorption. An —OH group shows a more intense absorption

band than an N—H bond because the —OH bond is more polar (Nguyen et al., 2012).

The FTIR spectrum confirms the L-lysine immobilization on PVDF surface by the affirmation of bands in the 3200–3400 cm^{-1} region, justifying the L-lysine/PAA/PVDF characteristic.

3.1.2. The High Resolution Scanning Electron Microscopy (HRSEM)

Results from HRSEM characterization showing the surface morphology of the respective membranes are reported in Fig. 2a–d.

Fig. 2 shows the HRSEM images of the PVDF microfiltration membranes without Ni/Fe and with Ni/Fe nanoparticles. The surfaces of four membranes showed the pore sizes of the membranes which were clearly observed. When bare PVDF membranes were coated with acrylic acid, there was no significant change on the surface of the composites Fig. 2b. However, ATR-FTIR proved that the composition of the membrane was altered when the —COOH functional groups were introduced to the surface of the membranes. Several small protrusions appeared when the PAA/PVDF was coated with the L-lysine indicating the attachment of the amino groups on the surface of the membrane. The pore size of the L-lysine/PAA/PVDF composite decreased as compared to the bare membrane and the PAA/PVDF modified membrane. Several small groves appeared when the L-lysine/PAA/PVDF membranes were introduced into the aqueous solutions containing metal ions and sodium borohydride as a reducing agent. The spherical shaped nanoparticles on the membrane's surface indicated the successful immobilization of bimetallic Ni/Fe nanoparticles.

3.1.3. FESEM-EDS characterization

The results of SEM-EDS analysis in Fig. 3 show that Fe and C were the main constituents of fresh Ni/Fe/L-lysine/PAA/PVDF composite. The Fe particles ranged from 20 to 30 nm in size whereas the sizes of Ni layers were in range12–18 nm. To further understand the patterns of Ni and Fe species in the membrane, an O atom was observed in Fig. 3 and this was due to the formation of an oxide layer on core–shell particles surface during synthesis. A Na peak was observed because of the unreacted remainder of Na during the ion exchange process. However a Boron peak was not observed indicating that Boron atoms were removed thoroughly during the rinsing step with ethanol (initially introduced to the membrane during reduction processes).

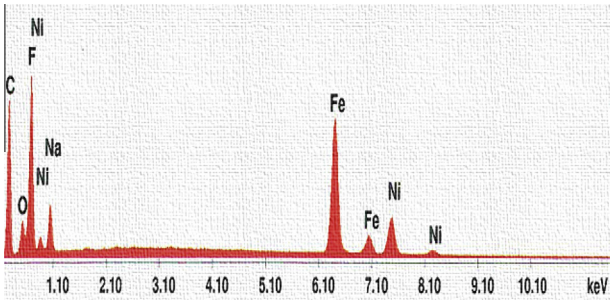

Fig. 3. SEM-EDS spectra of nanoscale Ni/Fe in L-lysine/PAA/PVDF composite.

3.1.4. Cross-sectional images of a bare PVDF membrane and Ni/Fe/L-lysine/PAA/PVDF composite

The cross-sectional images of a Bare PVDF membrane and Ni/Fe/L-lysine/PAA/PVDF composite were obtained. The results of HRSEM are presented in Fig. 4.

In this study, complete membrane pore filling might not be desirable because of the high diffusion resistance for the hydrophobic chlorinated organic molecules and also for nanoparticle synthesis. The cross-sectional images of bare PVDF membrane and Ni/Fe/L-lysine/PAA/PVDF composite are shown in Fig. 4. By contrast, different regions of the cross sections clearly show the structural difference between the L-lysine/PAA/PVDF modified membrane (B) and the unmodified substrate membrane (A). As shown in Fig. 4A and B, the bare PVDF has a sponge-like image suggesting that during the membrane preparation the casting solution had high viscosity as compared to the finger like membrane where the solution was less viscous. The pores inside the L-lysine/PAA/PVDF substrate are filled with small grains of Ni/Fe nanoparticles, suggesting that Ni/Fe nanoparticle immobilization has taken place throughout the pores of the PVDF substrate.

3.1.5. TEM characterization

The solution phase images of the Ni/Fe nanoparticles were obtained. The results of TEM obtained are presented in Fig. 5.

Fig. 5 shows the HRTEM images of NiFe nanoparticles which were synthesized in methanol medium using an initial Fe: Ni molar ratio of 1:4. These nanoparticles are black in color and have a

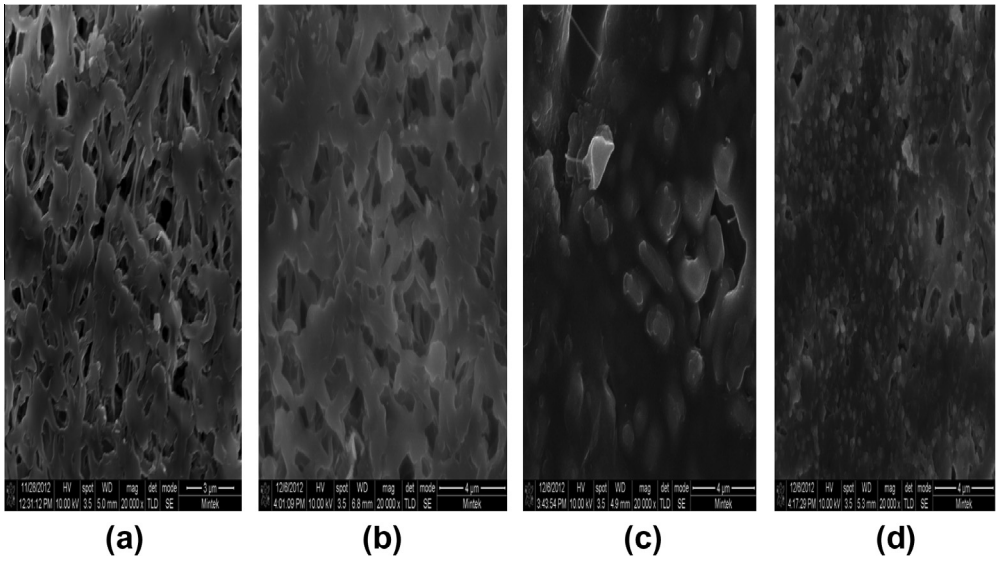

Fig. 2. (a–d) HRSEM images of microfiltration membranes in the absence and presence of Ni/Fe nanoparticles. (a) Bare PVDF, (b) PAA/PVDF, (c) L-lysine/PAA/PVDF, (d) Ni/Fe nanoparticles in L-lysine/PAA/PVDF membrane.

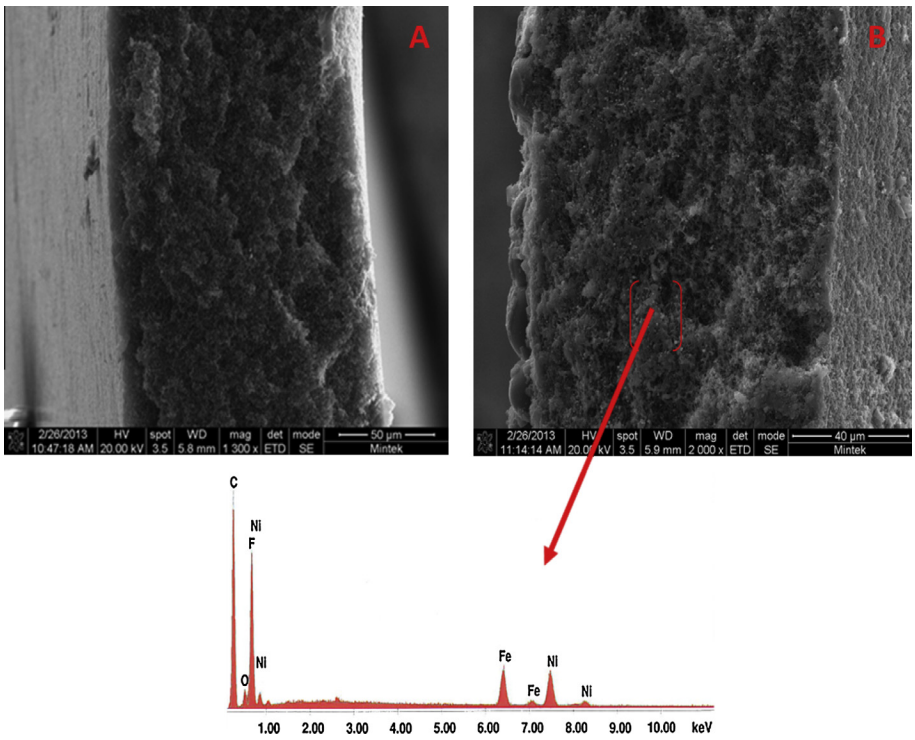

Fig. 4. HRSEM cross-sectional images of a bare PVDF (A) membrane and Fe–Ni/L-lysine/PAA/PVDF composite (B).

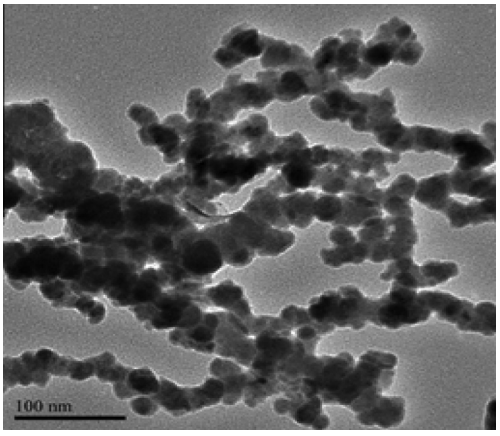

Fig. 5. HRTEM image of the freshly synthesized solution phase of bimetallic Ni/Fe nanoparticles.

spherical morphological shape and are closely packed towards each other indicating their agglomeration in the absence of a surfactant. In addition, they exhibited a wide size distribution 20–30 nm. The purpose for the synthesis of these unsupported nanoparticles was to contrast them to the nanoparticles embedded on the L-lysine–PAA–PVDF composite. The agglomeration of the unsupported nanoparticles had previously been reported to be attributed by magnetic interactions between the primary metal particles (Yuvakkumar et al., 2011). It has been suggested that the porous, nanocrystalline morphology results in high levels of stepped surfaces and increases their reactivity (Yuvakkumar et al., 2011). Therefore in this report we discuss about the nanoparticles being entrapped in the modified PVDF membrane the surfactant.

It is noteworthy to observe that the morphology of Ni/Fe nanoparticles on the L-lysine/PAA/PVDF membranes showed some differences as compared to the unsupported bimetallic Ni/Fe nanoparticles shown in Fig. 5. The agglomeration of unsupported Ni/Fe nanoparticles was observed in Fig. 5. In contrast, a relatively uniform size distribution of spherical Ni/Fe nanoparticles was observed in the L-lysine/PAA/PVDF membranes in Fig. 2d and this indicated a low agglomeration of immobilized nanoparticles due to the available functional groups provided by the L-lysine.

This is consistent with the literature provided by Bhattacharyya et al. (2011). The interaction between L-lysine and metal particles may involve several interaction mechanisms including ion exchange, chelation and electrostatic interaction. The monomer units of L-lysine/PAA/PVDF membranes contain diamine and adipic acid, which can serve as chelating agents for ferrous ions. The zero valent nanoparticles would be then well-dispersed after the addition of $NaBH_4$, leading to the decrease in agglomeration of Ni/Fe nanoparticles.

3.1.6. Contact angle measurement

The contact angle measurement is an instrument that is used to investigate the hydrophilicity and hydrophobicity of a substance. Contact angle values for bare PVDF, PAA/PVDF, L-lysine–PAA–PVDF and Fe–Ni/L-lysine–PAA–PVDF membranes are reported in Table 1.

A value of 60.3° for the bare membrane was observed due to the fact that the commercial PVDF membrane already had some degree of wetting arising from the presence of 2-methoxyethanol employed as a preservative. Thus the PAA/PVDF show some decrease in contact angle value of 43.0 ± 3.8 as compared to the unmodified

Table 1
Contact angle values for bare PVDF, PAA/PVDF, L-lysine–PAA–PVDF and Fe–Ni/L-lysine–PAA–PVDF membranes.

Membrane	Contact angle (θ_c)	Surface energy (N/m)
Bare membrane	60.3 ± 5.0	80.64
PAA–PVDF (modified)	43.0 ± 3.8	136.35
L-lysine–PAA–PVDF (modified)	37.0 ± 3.8	145.32
Ni/Fe composite	39.3 ± 4.6	139.01

membrane. The carboxyl functional groups presented by the PAA on the surface of the membrane increased the membrane's hydrophilicity. The modified L-lysine/PAA/PVDF membrane also had a decreased contact angle of 37.0 ± 3.8 confirming a significant upturn degree of wetting due to the presence the carboxylic group and amine (hydrophilic property). The composite with the Ni/Fe nanoparticles had a slight increase of the contact angle of 39.3 ± 4.6 due to the presence of the nanoparticles upon the surface and inside the pores of the membranes.

3.1.7. XRD characterization

XRD is a non-destructive technique that reveals detailed information about the chemical composition and crystallographic structure of the substance. The results of the X-ray diffraction patterns obtained for modified membranes are presented in Fig. 6.

The results show the XRD patterns of the nanoparticles inside the composite after reduction for 10 min by a reducing agent sodium borohydride at ambient temperatures. The XRD patterns were recorded at 2θ range for the reduced zerovalent bimetallic Ni/Fe nanoparticles inside the membrane. From the integration of the area under the crystalline peaks, it can be seen that the composite contains predominantly major crystalline peaks at the 2θ values of 18.6°, 20.3°, and 27° that are attributed to the PVDF membrane as the surfactant (Ataollahi et al., 2012). For Ni/Fe nanoparticles the peak concentration of the metal ions was observed between 40.9° and 45° indicating the adherence of the zero valent bimetallic nanoparticles unto the surface of the membrane (Xinghua and Chengwen, 2012). The XRD measurements give evidence of the existence of the alloy in the modified membrane due to the observed reflection peaks at 56° and at 70° attributed to the Ni and Fe ions, respectively.

In order to quantify the attached metals on the membrane, our study was carried by immersing one Fe–Ni/L-lysine/PAA/PVDF composite containing Ni/Fe particles into 10 mL concentrated nitric acid for a duration of 1 h. It was observed that the color of composite changed from black to white, while the color of nitric acid solution changed from white to greenish light-brown, suggesting that Fe and Ni nanoparticles were dissolved in the nitric acid. This indicates that the anchored nanoparticles were stripped off by the strong acid from the structure of the membrane. In order to quantify the metal content anchored within the structure of the Fe–Ni/L-lysine/PAA/PVDF composite, the analysis was carried out using inductively coupled plasma atomic emission spectroscopy (ICP-OES). Based on the ICP-OES analyses, each 47 mm L-lysine/PAA/PVDF membrane contained approximately 10.1 mg Fe and 2.43 mg Ni.

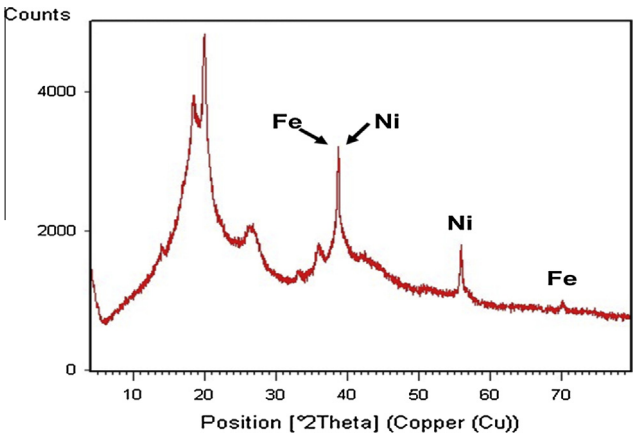

Fig. 6. XRD patterns of Fe–Ni nanoparticles synthesized in L-lysine/PAA/PVDF composite.

3.2. Application studies of Fe–Ni/L-lysine/PAA/PVDF membrane for catalytic dechlorination of PCB77 in water

In a Ni/Fe bimetallic system, the role of Fe (reactant) in zero valent form is to generate hydrogen (near neutral pH operation) via corrosion reaction. Ni acts as a hydrogenation catalyst and thus can be considered as providing the active sites in the bimetallic system. The Ni surface coverage (assuming uniform deposition of Ni on the Fe-modified membrane) on bimetallic particles can be estimated on the basis of 30 nm particle size and a Ni cross-sectional area of 0.0787 nm^2 (Bhattacharyya et al., 2011).

During the 9 h dechlorination process at ambient conditions as shown in Fig. 7, it was observed that the degradation of PCB77 by the Ni/Fe nanoparticles occurred through the formation of less chlorinated biphenyl. It has been proven in the literature that non-*ortho*-chlorinated PCB congeners dechlorinate faster than the *ortho*-chlorinated isomers. The reactivity of the chlorine substituents decreases in the order *para* ≈ *meta* > *ortho* (Ambati et al., 2012). During the 9 h, the experiment achieved a 98% dechlorination effiency. Based on the conditions which the study was carried it was evident that high percentages of non-toxic biphenyl can be achieved in longer times as compared to other expensive sets of conditions which dechlorinate the PCB77 at 75–80% dechlorination efficiencies for 2 h (Parshetti and Doong, 2012).

Based on the assumption provided by Parshetti and Doong when they were assessing the leaching of the nanoparticles from polyethylene glycol-grafted microfiltration membranes preformed composites (Parshetti and Doong, 2012), they found out that the leaching of the nanoparticles occurred mostly in PEG/PVDF membrane as compared to PEG/nylon 66. The nylon 66 membrane was found to be a more efficient support than the PVDF membrane for trichloroethylene (TCE) hydrodechlorination, because of its high multifunctional chelating sites which can reduce the agglomeration and retain high Ni content of Ni/Fe. The monomer units of the L-lysine/PAA/PVDF membrane are methylenediamine and adipic acid. This means that L-lysine/PAA/PVDF membrane has multifunctional chelating groups to complex metal ions. resulting in minimization of the agglomeration of the bimetallic nanoparticle which leads to their leaching. Fig. 7 shows the reactivity of Ni/Fe nanoparticles toward PCB77 dechlorination under room conditions. The original concentration of PCB77 before dechlorination was 4.90×10^{-2} mM. After dechlorination by Ni/Fe nanoparticles immobilized in PVDF membranes, the remaining concentration was 9.9×10^{-4} mM translating to 98% dechlorination efficiency within 9 h. Thus the membranes exhibited a high reactivity toward PCB77 dechlorination.

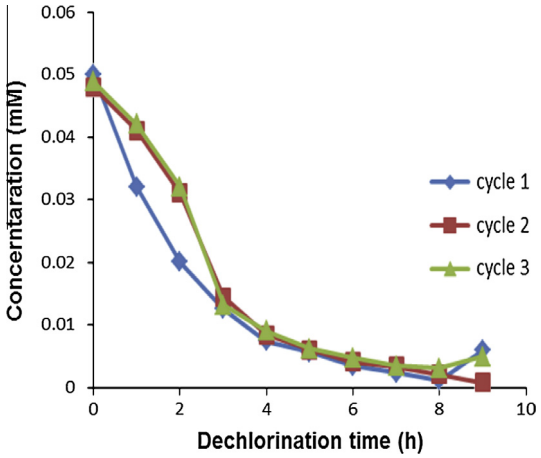

Fig. 7. PCB77 conversion to non-toxic biphenyl with in 9 h reaction time in batch mode (pH 6.6) for 3 different cycles using the same Fe–Ni/L-lysine/PAA/PVDF membrane (17.3 cm^2 external area).

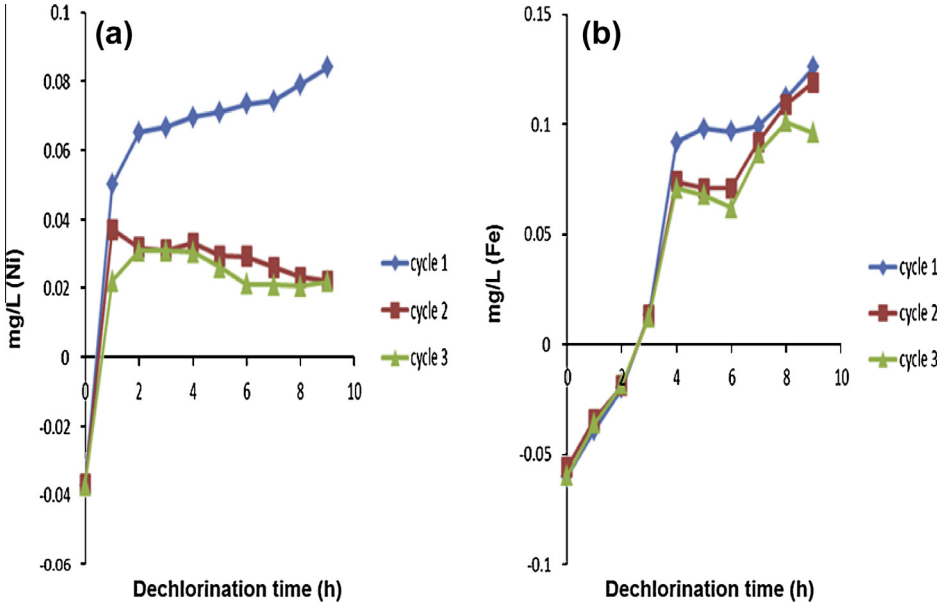

Fig. 8. (a) Concentration of Ni content during a 3 turn cycle of dechlorination. (b) Concentration of Fe content during a 3 turn cycle of dechlorination.

As indicated in Fig. 8a it was observed that the presence of Ni content inside the lysine/PAA/PVDF membrane was still in relatively high percentage due to the availability of the multi-chelating sites which prevents the leaching. Cycle 1 had a high Ni leaching concentration (3.4%) and this was assumed to be the cause of the unreacted Ni nanoparticles on the surface of the formed composite. However after 2 and 3 cycles it was observed that the leaching occurred at very low percentages of about ~2% indicating a strong interaction between the membrane and the nanoparticles.

The interaction between metal cations and carboxylic and amine groups in L-lysine is critical in the prevention of particle aggregation, which can greatly influence the nanoparticle size. The interaction mechanisms consist of ion exchange, chelation and electrostatic binding.

In Fig. 8b it was noticed that the Fe leaching occurred at very low concentrations, about 0.9% of the original solution during the first, second and third cycles. This observation indicated that during the ion-exchange process mentioned in Section 2.4 the Fe^{2+} were strongly bound to the $—COO^-$ groups hence the leaching of Fe atoms was minimized due to their good dispersion on the membrane with less agglomeration. The aggregation of Fe atoms was reduced by the availability of amines and carboxylic groups provided by the L-lysine monomer and hence the leaching was maintained at low concentrations due to the electrostatic binding of the nanoparticles on the available functional groups.

4. Conclusions

In this study, we have demonstrated a simple approach for the immobilization of the bimetallic Ni/Fe nanoparticles inside the PVDF microfiltration membranes using thermal grafting polymerization of PAA and L-lysine which was covalently bonded to the polymerized acrylic acid chains with the aid of a water-soluble EDC.

The Ni/Fe nanoparticles were uniformly immobilized in the membrane with minimal particle agglomeration observed. The L-lysine–PAA–PVDF composite was found to be an efficient catalyst for PCB77 hydrodechlorination because of its high multifunctional chelating sites which can reduce agglomeration and retain high content of Ni/Fe nanoparticles. Degradation of 98% (starting concentration of 4.95×10^{-2} mM and remaining un-dechlorinated concentration of 9.9×10^{-4} mM) of the PCB77 was achieved within 9 h by the immobilized Ni/Fe nanoparticles in L-lysine–PAA–PVDF membrane. The leaching of the Ni was observed to be higher than that of the Fe metal. The leaching of the Ni content during the first cycle was 3.4% of the initially retained Ni on the membrane. However after 2–3 cycles it was observed that the leaching decreased to about ~2%. The relatively high amount of Ni leached during the first cycle could be explained by the presence of unreacted Ni which is loosely attached on the outer surface of the membrane and hence easily washable. In the subsequent cycles, the unreacted Ni is nearly completely removed, hence the decreasing amounts observed.

The Fe leaching occurred at very low amounts (~0.9%) as compared to Ni content. Results obtained in this study clearly indicate that the immobilized Ni/Fe nanoparticles in L-lysine–PAA–PVDF microfiltration membranes are environmentally safe to use as they do not leach out hazardous metals into the treated water during dechlorination of chlorinated hydrocarbons.

References

Ambati, J., Song, Y., Lehmler, H.J., 2012. Density functional theory study of semiquinone radical anions of polychlorinated biphenyls in the syn- and anti-like conformation. J. Phys. Chem. Earth 6, 1588–1595.
Andersin, J., Parkkinen, P., Honkala, K., 2012. Pd-catalyzed hydrodehalogenation of chlorinated olefins: theoretical insights to the reaction mechanism. J. Catal. 290, 118–125.
Ataollahi, N., Ahmad, A., Hamzah, H., Rahman, M.Y.A., Mohamed, N.S., 2012. Preparation and characterization of PVDF–HFP/mg49 based polymer blend electrolyte. Int. J. Electrochem. Sci. 7, 6693–6703.
Behari, J., 2010. Principles of nanoscience: an overview. J. Exp. Biol. 48, 1008–1019.
Berger, M., Finkbeiner, M., 2010. Water footprinting: how to assess water use in life cycle assessment? Sustainability 2, 919–944.
Bhattacharyya, D., Smuleac, V., Varma, R., Sikdar, S., 2011. Green synthesis of Fe and Fe/Pd bimetallic nanoparticles in membranes for reductive degradation of chlorinated organics. J. Membr. Sci. 379, 131–137.
Bieroza, M.Z., Bridgeman, J., Baker, A., 2010. Fluorescence spectroscopy as a tool for determination of organic matter removal efficiency at water treatment works. Drink-Water Eng. Sci. 3, 63–70.
Ezzaafrani, M., Ennaciri, A., Harcharras, M., Khaoulaf, R., Capitelli, F., 2012. Crystal structure and infrared spectrum of new magnesium tetra-ammonium cyclotriphosphate tetrahydrate $Mg(NH_4)4(P_3O_9)_2\cdots4H_2O$. Z. Kristallogr. 227, 141–146.

Gao, J., Yu, J., Li, C., 2010. Chemical modification of polyvinylidene fluoride (pvdf) membrane and its application to milk purification. Inter. J. Nonlinear Sci. Numer. Simul. 11, 37–41.
Grzelczak, M., Vermant, Furst, E.M., iz-Marz n, M., 2010. Directed self-assembly of nanoparticles. ACS Nano 4, 3591–3605.
Gui, M., Smuleac, V., Ormsbee, L., Sedlak, D., Bhattacharyya, D., 2012. Iron oxide nanoparticle synthesis in aqueous and membrane systems for oxidative degradation of trichloroethylene from water. J. Nanopart. Res. 14, 1–16.
He, Y.Q., Chen, H.B., Sun, H., Wang, X.D., Gao, J.P., 2012. A pH and electric responsive graphene oxide based composite hydrogel. Adv. Mater. Res. 430, 327–330.
Hoekstra, A.Y., 2012. The hidden water resource use behind meat and dairy. J. Webster Ed. Earthscan 2, 3–8.
Hoekstra, A.Y., Mekonnen, M.A., Chapagain, A.K., Mathews, R.E., Richter, B.D., 2012. Global monthly water scarcity: blue water footprints versus blue water availability. Plos One 7 (2), e32688.
Huh, K., Kang, H., Lee, Y., Bae, Y., 2012. PH-sensitive polymers for drug delivery. Macromol. Res. 20, 224–233.
Li, S., Fang, Y.-L., Romanczuk, C.D., Jin, Z., Li, T., Wong, M.S., 2012. Establishing the trichloroethene dechlorination rates of palladium-based catalysts and iron-based reductants. Appl. Catal. B 25, 95–102.
Mackenzie, K., Bleyl, S., Georgi, A., Kopinke, F.D., 2012. Carbo–iron – an Fe/Ac composite – as alternative to nano-iron for groundwater treatment. Water Res. 46, 3817–3826.
Man, J.H., Garry, N.B.B., Bumsuk, J., 2011. Effect of surface charge on hydrophobically modified poly(vinylidene fluoride) membrane for microfiltration. Desalination 270, 76–83.
Nguyen, J., Reul, R., Roesler, S., Dayyoub, E., Schmehl, T., Gessler, T., Seeger, W., Kissel, T.H., 2012. Amine-modified poly(vinyl alcohol)s as non-viral vectors for sirna delivery: effects of the degree of amine substitution on physicochemical properties and knockdown efficiency. Pharm. Res. 12, 2670–2682.
Parshetti, G.K., Doong, R., 2012. Dechlorination of chlorinated hydrocarbons by bimetallic Ni/Fe immobilized on polyethylene glycol-grafted microfiltration membranes under anoxic conditions. Chemosphere 86, 392–399.
Pfister, S., Saner, D., Koehler, A., 2011. The environmental relevance of water consumption in global power production. Int. J. Life Cycle Ass. 16, 580–591.
Ramezani-Dakhel, H., Mirau, P.A., Naik, R.R., Knecht, M.R., Heinz, H., 2013. Stability, surface features, and atom leaching of palladium nanoparticles: toward prediction of catalytic functionality. Chem. Phys. 15, 5488–5492.
Ridoutt, B.G., Pfister, S., 2010a. Reducing humanity's water footprint. Environ. Sci. Technol. 44, 6019–6021.
Ridoutt, B.G., Pfister, S., 2010b. A revised approach to water footprinting to make transparent the impacts of consumption and production on global freshwater scarcity. Glob. Environ. Change 20, 113–120.
Ruhl, A.S., Ünal, N., Jekel, M., 2012. Evaluation of two-component Fe(0) fixed bed filters with porous materials for reductive dechlorination. Chem. Eng. J. 209, 401–406.
Saha, M.S., Paul, D.K., Peppley, B.A., Karan, K., 2010. Fabrication of catalyst-coated membrane by modified decal transfer technique. Electrochem. Commun. 12, 410–413.
Seol, S.K., Kim, D., Jung, S., Hwu, Y., 2011. Microwave synthesis of gold nanoparticles: effect of applied microwave power and solution pH. Mater. Chem. Phys. 131, 331–335.
Smuleac, V., Bachas, L., Bhattacharyya, D., 2010. Aqueous-phase synthesis of PAA in PVDF membrane pores for nanoparticle synthesis and dichlorobiphenyl degradation. J. Membr. Sci. 346, 310–317.
Su, Y., Hsu, C.Y., Shih, Y., 2012. Effects of various ions on the dechlorination kinetics of hexachlorobenzene by nanoscale zero-valent iron. Chemosphere 88, 1346–1352.
UN-Habitat., 2011. Cities and Climate Change — Global Report on Human Settlements. Available on-line at http://www.unhabitat.org/content.asp?typeid=19&catid=555&cid=9272.
UN-Water Global Analysis and Assessment of Sanitation and Drinking-Water., 2012. Available on-line at http://www.un.org/waterforlifedecade/pdf/glaas_report_2012_eng.pdf.
Verones, F., Hanafiah, M.M., Pfister, S., Huijbregts, M.A.J., Pelletier, G.J., Koehler, A., 2010. Characterisation factors for thermal pollution in freshwater aquatic environments. Environ. Sci. Technol. 44 (24), 9364–9369.
WHO and UNICEF, 2012. Progress on drinking water and sanitation. Available online at http://www.unicef.org/media/files/JMPreport2012.pdf.
Xinghua, S., Chengwen, Q., 2012. Influence of pH and bath composition on properties of Ni–Fe alloy flms synthesized by electrodeposition. Bull. Mater. Sci. 3 (2), 183–189.
Yoshimatsu, K., Lesel, B.K., Yonamine, Y., Beierle, J.M., Shea, K.J., 2012. Temperature-responsive "catch-and-release" of proteins using multifunctional polymer nanoparticles. Angew. Chem. Int. Ed. 10, 2405–2408.
Yunqing, Z., Xie, Q., Fengjiao, C., Xinfei, F., Yujie, F., 2012. CeO_2–TiO_2 coated ceramic membrane with catalytic ozonation capability for treatment of tetracycline in drinking water. Sci. Am. 4, 1191–1199.
Yuvakkumar, R., Elango, V., Rajendran, V., Kannan, N., 2011. Preparation and characterization of zero valent iron nanoparticles. Dig. J. Nanomater. Biosci. 4, 1771–1776.